Trans Indian Inst Met (2019) 72(10):2753–2761
https://doi.org/10.1007/s12666-019-01752-7

TECHNICAL PAPER

Effect of Oxide Fluxes in Activated TIG Welding of Stainless Steel 316LN to Low Activation Ferritic/Martensitic Steel (LAFM) Dissimilar Combination

Naishadh P. Patel[1] · Vishvesh J. Badheka[2] · Jay J. Vora[2] · Gautam H. Upadhyay[3]

Received: 23 November 2018 / Accepted: 5 June 2019 / Published online: 21 June 2019

Abstract The aim of current work is to study the effect of different oxide fluxes in activated TIG welding process of dissimilar welding between LAFM and 316LN on weld dimensions, macro- and microexamination, and microhardness. Different oxide fluxes, namely TiO_2, Fe_2O_3, CuO, Co_3O_4, and HgO, were used for the experiment, and its results were compared with convention TIG welding. Flux paste was applied over the area to be welded using a paint brush at the middle portion of the specimen. All welding experiments were carried out on a bead on a plate and under the same welding conditions and parameters. The experimental result reveals that full-length penetration was achieved with the use of Co_3O_4 and TiO_2 fluxes. This enhancement in depth of penetration is attributed to the reverse Marangoni effect and arc constriction mechanism. In this study, insight was also revealed pertaining to the depth-enhancing mechanism present during ATIG welding of LAFM and SS316LN joints.

✉ Naishadh P. Patel
naishadh.patel27@gmail.com

Vishvesh J. Badheka
vishvesh79@gmail.com

Jay J. Vora
vorajaykumar@gmail.com

Gautam H. Upadhyay
gautam.upadhyay@gmail.com

[1] Metallurgy Department, L. E. College, Morbi, India

[2] Department of Mechanical Engineering, School of Technology, Pandit Deendayal Petroleum University, Raisan, Gandhinagar 382007, India

[3] D. A. Degree College of Engineering and Technology, Mahemdabad, India

Keywords A-TIG · Dissimilar · Welding

1 Introduction

High alloy steel materials such as 9–12 Cr steels were favored choice for use in structural materials for fusion reactor and high-performance power plants; however, change in phase stability and microstructural properties under radiation atmosphere leading to hydrogen embrittlement were two major issues faced by the designers. Added to it, in the present scenario, dumping, recycling and decommissioning of the components of equipment in nuclear service are also a major issue [1]. Thus, the steel selected as a structural material should have minimum activation at the end of its service to enable shallow land burial; 9–12 Cr steels are ruled out due to the same reason. These steels are termed as reduced activation ferritic/martensitic (RAFM) steels or low activation ferritic/martensitic (LAFM) steels and are developed by altering the chemical composition of modified 9Cr-1Mo (grade 91, ASME Sec II) by replacing Mo and Nb with W and Ta, respectively, to acquire minimum activation [2–4]. Elements like Cu, Mn, P, B, and S which causes induced activity are also specified at a lower level for this steel [5–10]. On the other hand, austenitic stainless steel grade 316LN has been used in the clad and wrapper of Fast Breeder Test Reactor (FBTR) [11, 12] due to its excellent corrosion resistance which is a need in nuclear equipment.

The general predicament in welding of the equipment parts used in nuclear service is that, there should be minimum number of welds which ultimately reduce the volume of weld metal and HAZ. This rules out the possibility of using conventional welding processes such as gas metal arc welding, metal active gas, shielded metal arc welding,

and submerged arc welding which is high heat input processes. The favorable processes are tungsten inert gas welding, electron beam welding, narrow gap tungsten inert gas, and laser beam welding [12–14]. The basic design for lead–lithium ceramic breeder (LLCB) TBM essentially consists of an intricate box structure with different subcomponents like first wall (FW), ceramic breeder cassettes, top and bottom cap plates, vertical stiffeners and flow dividers, inlet and outlet pipes for Pb–Li, inner and outer back plates, etc. The main application of the dissimilar weld between LAFM and 316 LN steel is for the connection of the test blanket module (TBM) to the supply systems of the International Thermonuclear Experimental Reactor (ITER) [6]. Dissimilar joints always pose a challenge to the fabricators especially in welding as they have different physical and melting properties.

The TIG welding process is one of the most sought processes where high-quality joints are required. However, its limited penetration capability, particularly in single-pass autogenous operations, limits the use of this technology [14, 15]. In addition to this, NG-TIG, a variant of the process, require better accessibility of weld joint and special preparation of weld edge. The use of a high vacuum chamber in EBW processor and LBW process adds high equipment cost and restricts the onsite welding. Activated tungsten inert gas (ATIG) welding process, another variant of the TIG process, was first developed by Paton Electric Welding Institute in the 1960s [16]. In this process, a chemical powder (termed as flux) is applied on the plate surface before welding. Flux is generally in powdered form and mixed with a carrier solution like acetone, methanol, or ethanol to make a fine paste. This paste is then applied with the help of a paintbrush at the faying surfaces to be welded [16]. Flux particles get vaporized at arc temperatures and play an important role in initiating the reverse Marangoni effect. The process has reported an increase in penetration up to 300% as compared to the TIG welding process. Thus, it enables single-pass welding of higher thickness plates with higher welding speed and hence reduces heat input.

ATIG welding of the dissimilar joint between 316LN and LAFM also possesses challenges due to difference in chemical composition, thermal and electrical conductivity, and large thermal stresses generated due to the difference in thermal expansion characteristics of two steels and asymmetric weld [6, 17]. There is literature available indicating the use of oxide fluxes in the ATIG welding process. Tseng and Hsu [18] studied the performance of activated TIG process using TiO_2, MnO_2, SiO_2, Al_2O_3, MoO_3 in austenitic stainless steel weld and concluded that SiO2 and MoO3 fluxes achieve an increase in weld depth and a decrease in bead width, respectively, which leads to higher penetration compared to TIG. Vora and Badheka [19–22] have highlighted the effect of different oxide fluxes CaO, Fe_2O_3, MnO_2, TiO_2, ZnO, Al_2O_3, Co_3O_4, CuO, HgO, MoO_3, and NiO on LAFM steel and have confirmed the increase in penetration compared to conventional TIG welding process; however, full penetration is achieved in case of Fe_2O_3, TiO_2, Co_3O_4, and CuO due to combined effect of arc constriction and Marangoni mechanism.

Although there are good works of the literature that are available on ATIG welding of RAFM and 316L stainless steel separately, very few works of the literature are available in public domain for dissimilar weld between RAFM and 316LN using ATIG Process. Albert et al. [6] studied the mechanical properties of similar and dissimilar weldments of RAFMs and AISI 316L(N) SS by the EBW process. They concluded a detailed study of mechanical properties in the case of dissimilar welding before direct joint between LAFMs and AISI 316L(N) SS using EB welding. Another study by Vidyarthy et al. [13] on dissimilar ATIG welded P91 to 316L has been reported to analyze the structure–property relation in which they have successfully welded 316L–P91 using ATIG process and satisfactory results of mechanical and metallurgical properties have been found. However, to the best of our knowledge, until now the effect of oxide fluxes on a dissimilar weld between LAFM and 316 LN using the ATIG process has not been reported yet.

Different oxide fluxes have individual effects on different types of materials used for welding. Although fluxes used for experimental work have already been utilized for earlier research work by a different researcher, these are either for similar joining of metals or with different welding process or processes [6, 19, 20, 23, 24]. Hence, it is necessary to analyze the effect of these fluxes on the proposed dissimilar metal joining combination. In the present study, an effort was made to analyze the effect of five different oxide fluxes such as TiO_2, Fe_2O_3, CuO, Co_3O_4 and HgO in ATIG welding of the dissimilar joint between LAFM and 316LN on weld bead attributes and mechanism responsible for the change in deeper penetration. Efforts have also been made to analyze the effect of microstructures and microhardness for weld joint integrity.

2 Materials and Methods

2.1 Base Metal

The chemical composition of 6-mm-thick LAFM steel and SS 316LN used as a base material for the present investigation is shown in Table 1. LAFM steel was hot-rolled, quenched and tempered. LAFM and AISI 316LN base plates of size 100 mm × 22 mm × 6 mm were taken for experimental trials.

Table 1 Chemical composition of LAFM steel and 316LN steel

Elements	C	Si	Mn	P	S	Cr	Mo	Ni	Ti	Co
LAFM	0.1	0.02	0.54	0.003	0.002	9.0	< 0.002	< 0.005	< 0.005	< 0.005
316LN	0.026	0.59	1.85	0.030	0.013	17.65	2.89	12.23	–	–

Elements	V	W	Ta	B	Al	Cu	O	N	Nb	As + Sn + Sb + Zr
LAFM	0.23	1.42	0.15	< 0.0001	0.008	< 0.002	0.09	0.025	< 0.001	< 0.03
316LN	–	–	–	–	–	–	–	0.11	–	–

Table 2 Flux and its weight calculation

Flux	Color identification	Length of Strip (mm)	Width (mm)	Flux height (mm)	Density (gm/mm^3)	Weight of flux (gm)
TiO_2	White	100	10	0.15	0.00423	0.634
Fe_2O_3	Dark Red	100	10	0.15	0.00524	0.786
CuO	Black	100	10	0.15	0.00631	0.946
Co_3O_4	Black	100	10	0.15	0.00611	0.916
HgO	Orange	100	10	0.15	0.01111	0.501

2.2 The Methodology of Flux Application

Five different oxide fluxes procured in powdered form were used for the experiments as shown in Table 2. Methanol was used as a carrier solvent to convert powder flux into a paste by mixing. Flux paste was applied over the area to be welded using a 10-mm-width paint brush moved in forward and backward direction at the middle portion of the specimen until all flux paste was consumed. The thickness of the flux layer was kept at 0.15 mm approximately (Calculation for the quantity of fluxes is shown in Table 2).

2.3 Experimental Setup for ATIG Welding

The experimental work was carried out in autogenous mode with Panasonic make GTAW power source having the capacity of 200 A with a 25% duty cycle and customized special purpose machine (SPM) for torch movement as shown in Fig. 1. Welding setup for experimental work using five different fluxes is shown in Fig. 1. Welding parameters used for all six experiments were chosen based on the previous work of Vora and Badheka [19, 20] shown in Table 3. The arc movement was in forward and backward direction in the central portion of the specimen to be welded. All experiments were carried out in flat position. Arc voltage measured was not a controllable parameter, and rests were controllable parameters. To measure peak temperature, K-type thermocouple was attached on the LAFM side and 316LN side by drilling a hole of 2 mm dia. and 3 mm depth approximately in case of ATIG using Co_3O_4 and normal TIG process. Also dissimilar material, RAFM to 316LN, was welded using the conventional TIG welding process to compare weld joint integrity with experiments carried out using five different fluxes on same dissimilar materials and parameters. After welding, visual inspection was carried out to check surface discontinuities like porosity, slag, crack, and incomplete fusion. Samples for macro- and microexamination were prepared using standard metallography techniques. The specimen was cut across the seam from the welded plate and rough ground on a surface grinder to make the surface of the specimen reasonably flat. Intermediate and fine polishing was carried out on emery papers of progressively finer grade (100, 220, 400, 600, 800, and fine polishing from coarse to fine). The polished samples were etched using Villella at the LAFM side and electroetching on the 316LN side. Additionally, macro features such as DOP, BW and HAZ were analyzed using the traveling/vernier microscope make: RADICAL Instrument available in PDPU laboratory. Further Vickers microhardness measurements were taken on a transverse cross-section specimen comprising of all zones of weldment at a regular interval of 0.5 mm using microhardness tester (Make: OMNITECH, Model: S Auto I). All measurements were taken at 1000 g load and 10 s dwell time. The facility of Vickers microhardness testing is available at Testing Laboratory of GEC, Gandhinagar.

3 Result and Discussion

3.1 Weld Bead Appearance

Figure 2 shows the front and back side of the TIG and ATIG weldments. It is observed that the surface

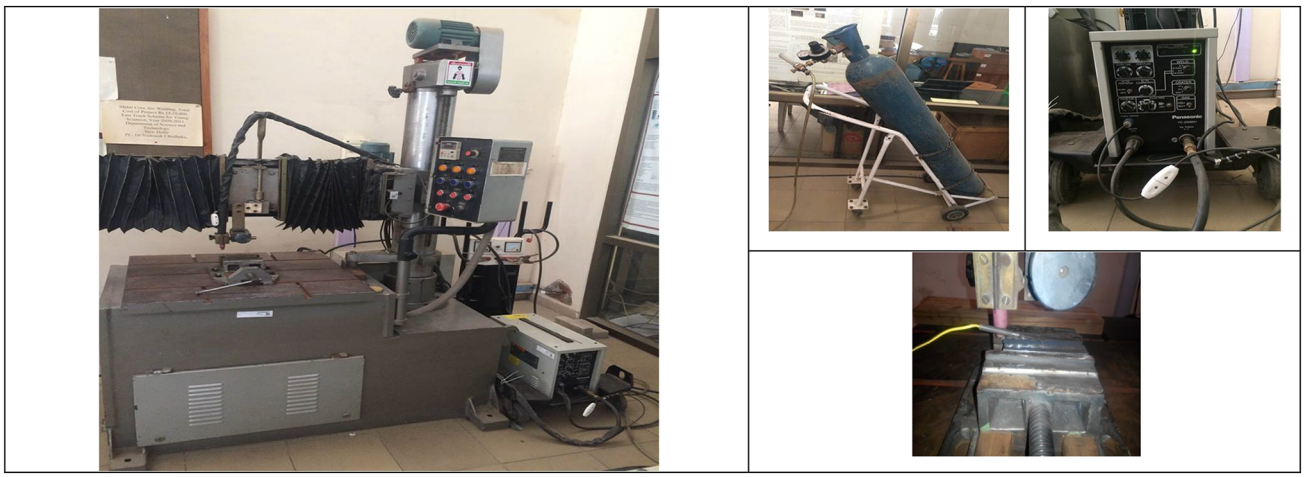

Fig. 1 Welding setup used for experimental work

Table 3 Welding parameters for all experiments

Polarity	DCEN
Type and diameter of electrode	W (2% thoriated) and 2.9 mm
Travel speed (mm/min)	100
Electrode angle	20°
Shielding	Argon (99.99%)
Gas flow rate	12–15 lpm
Electrode extension (mm)	5–6 mm
Stand-off distance (mm)	2–3 mm
Welding current (A)	200
Crater current (A)	200
Voltage (V)	15–16

appearance of TIG welded joint is more superior than ATIG welded joints. This is in line with the results reported by Chern et al. [25] and Kumar et al. [26]. This is due to spatter produced by slag residue. A small amount of spatter is observed on the bead surface with the use of flux Co_3O_4 in ATIG welding, whereas spatter-free bead surface is observed using conventional TIG welding and other oxide fluxes. This is attributed to slag layer forms due to the flux layer applied prior to welding in ATIG welding with other fluxes.

3.2 Effect of Oxide Flux on Weld Bead Dimensions and Macrostructure

Full-length penetration is observed in ATIG welded samples with the use of Co_3O_4 and TiO_2 flux, whereas there is no evidence of full penetration in conventional TIG and ATIG welded samples with the use of Fe_2O_3, CuO and HgO fluxes. The change in an arc shape and excessive spatter is attributed to stronger arc constriction mechanism which may be present in ATIG welding using Co_3O_4 and is absent in other fluxes. It can be confirmed by measuring peak temperature. Additionally, there is no evidence of depression or underfill in samples welded using the ATIG process with oxide flux as shown in Fig. 2. Moreover, a higher D/W ratio is achieved in ATIG welded samples compared to conventional TIG. However, the maximum depth-to-width ratio is achieved in the case of samples welded using Co_3O_4 and TiO_2 and minimum depth-to-width ratio is observed in the case of conventional TIG welded sample.

The measurement of weld bead dimensions has also revealed the presence of a mechanism for deeper penetration as the results shown in Fig. 3. The higher D/W ratio in the case of ATIG welded sample with the use of Co_3O_4 and TiO_2 compared to conventional TIG is due to the application of oxide flux. This is attributed to the mechanism of reverse Marangoni effect. However, penetration obtained in the case of the other three fluxes is lower compared to penetration achieved with Co_3O_4 and TiO_2 fluxes, which indicates the presence of additional mechanism apart from reverse Marangoni [20, 23, 27, 28]. It is confirmed in the macroexamination section.

Macrostructure of ATIG welded joints and TIG welded joint is shown in Fig. 4. TIG welded sample has shallow penetration while medium to deeper penetration is observed in case of ATIG welded samples. Additionally, samples welded using Co_3O_4 and TiO_2 flux show the highest penetration as well as narrow weld bead width as shown in Fig. 4. Although all experiments are taken at the same welding parameter and conditions, penetration and bead width are different for all cases. This is due to the presence of a reversed Marangoni effect [29–31] in which surface tension gradient at higher temperature results in the change in direction of fluid flow towards the center of the weld. As per Marangoni theory, with an increase in temperature of liquid weld metal, surface tension decreases

Conventional TIG	Front Surface	
	Back Surface	
ATIG welding with TiO_2 Flux	Front Surface	
	Back Surface	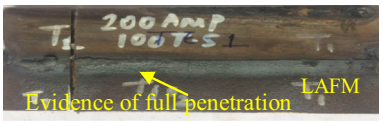
ATIG welding with Fe_2O_3 Flux	Front Surface	
	Back Surface	
ATIG welding with CuO Flux	Front Surface	
	Back Surface	
ATIG welding with Co_3O_4 Flux	Front Surface	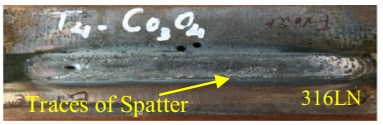
	Back Surface	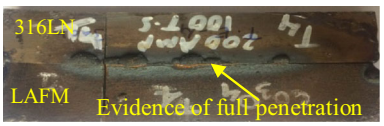
ATIG welding with HgO Flux	Front Surface	
	Back Surface	

Fig. 2 Front and back portion of weldments

which leads to a higher temperature at the center of weld metal compared to edges and therefore the direction of flow of liquid metal toward edges. This is the reason for the shallow and wide weld bead [32]. But oxygen in molten metal due to the use of oxide flux changes the relation between surface tension and temperature. So, with an increase in temperature of liquid weld metal, surface tension also increases, which leads to higher surface tension gradient at the center of the weld than edges at a higher temperature and therefore fluid flow towards center. This phenomenon is known as the reverse Marangoni effect.

As a result of this, higher D/W ratio is achieved in the case of Co_3O_4 and TiO_2, but the same effect is not observed with CuO, HgO, and Fe_2O_3 fluxes. These results suggest an additional mechanism responsible for deeper penetration other than reverse Marangoni mechanism. Weld bead shape can be predicted by arc shape. During ATIG, arc shape may have changed due to the use of oxide flux which results in arc constriction and leads to deeper penetration. However, only this confirmation is not the satisfying the presence of the arc constriction mechanism, and therefore, further discussion is explained in the next section.

3.3 Effect of Oxide Flux on Arc Voltage and Peak Temperature

The results of the oxide flux effect on arc voltage are shown in Table 4. As shown in Table 4, arc voltage increases when the ATIG process is carried out using Co_3O_4 and TiO_2 fluxes while for other fluxes, it remains the same. The arc voltage increases by approximately 0.5–1 V.

It is a fact that arc voltage is directly proportional to arc length and is kept constant in an autogenous mode of ATIG. But, an increase in voltage is observed in ATIG welding using Co_3O_4 and TiO_2 fluxes. It may be due to the oxide flux. Arc contains free electrons and positive ions which are generated due to the decomposition of flux. These cause attraction of free electrons which tends to constrict the arc. This happens only when the arc voltage increases. Thus, there is a presence of arc constriction mechanism with the use of Co_3O_4 and TiO_2 fluxes in TIG welding.

This can also be proved by measuring peak temperature. Peak temperature is measured in the case of ATIG with the Co_3O_4 and normal TIG welding process. Arc voltage variation is due to the different chemical composition of these fluxes. In the arc constriction mechanism, an increase in temperature at the anode is due to an increase in current density which results in an increase in peak temperature. As a result, a higher depth-to-width ratio is achieved. The same is observed in case of Co_3O_4 flux in which peak temperatures are 758 °C and 768 °C on LAFM and 316LN side, respectively, which are higher than normal TIG welding process (641 °C and 674 °C on LAFM and 316LN side, respectively). There is no variation in arc voltage in the case of ATIG welding with fluxes Fe_2O_3, HgO, and CuO which indicates the absence of arc constriction mechanism in these fluxes. The narrow HAZ is observed on the 316LN side as compared to the LAFM side. This can be attributed to higher thermal conductivity as compared to 316LN. The presence of arc constriction mechanism can be supported by the width of the weld bead and HAZ. The proposed mechanism can be supported by bead width results with the use of flux Co_3O_4 and TiO_2 in which bead width is reduced. There is marginal variation in bead width in case of ATIG welding with the use of fluxes Fe_2O_3, HgO, and CuO which indicates the absence of arc constriction mechanism in these fluxes, shown in Fig. 4.

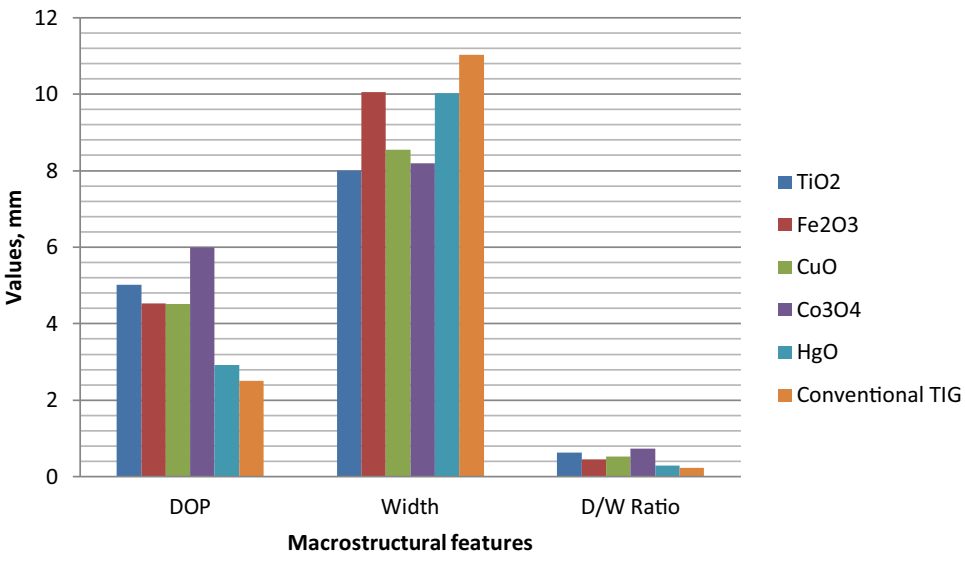

Fig. 3 Graphical representation of weld bead dimensions

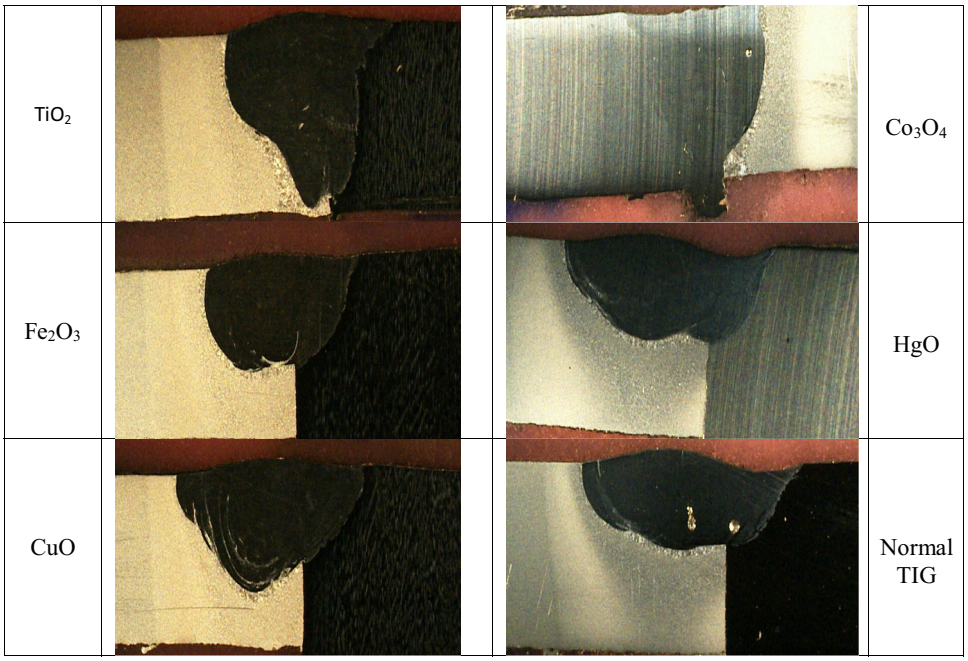

Fig. 4 Weld bead macrostructure of samples welded using ATIG (with flux) and conventional TIG (without flux)

Table 4 Effect of oxide fluxes on arc voltage

Process	ATIG with TiO_2	ATIG with Fe_2O_3	ATIG with CuO	ATIG with Co_3O_4	ATIG with HgO	Conventional TIG
Voltage (V)	15.5	15	15	16	15	15

3.4 Microexamination and Microhardness

The optical micrograph of RAFM to 316LN weldment is observed with 200X magnification. The microstructure of base metal LAFM consists of tempered lath martensite and has regular grains which are attributed to quenching and tempering effect in as-received condition of LAFM steel as shown in Fig. 5. It is a fact that insufficient cooling time/higher cooling rate in quenching leads to irregular grains which forms hard and lathy martensitic structure, whereas in tempering, lower cooling rate gives sufficient time to rearrange grains and therefore irregular grains are converted into rounded grains. It is also confirmed by the microhardness result of LAFM base metal as shown in Fig. 7.

316LN stainless steel consists of a fully austenitic structure. Similarly, the weld region as shown in Fig. 6 also experiences the same effect of quenching during welding. The higher cooling rates in fewer amounts of molten mass forms irregular grains of martensite due to insufficient time to form regular grains. Therefore, the lathy martensite structure is observed in the TIG welded sample and ATIG welded sample using TiO_2 flux except for samples welded using Co_3O_4. This may be due to the higher portion of 316LN in the weld region and also may be due to higher fraction delta ferrite in the weld. The same can be confirmed by hardness results.

The microstructure of the weld–LAFM HAZ interface of conventional TIG welded sample and ATIG welded samples using Co_3O_4 and TIO_2 are shown in Fig. 6. Coarse-grain structure is observed in LAFM HAZ–weld Interface because during weld thermal cycle, this region experiences higher temperature for a longer time with inherent precipitation of as-received LAFM steel completely dissolved in the matrix.

The microstructure of LAFM HAZ–LAFM base metal interface of conventional TIG welded samples and ATIG welded samples using Co_3O_4 and TIO_2 is shown in Fig. 6. Finer grain structure is observed at LAFM HAZ–LAFM base metal interface because this portion also experiences higher temperature, but for the shorter duration which results in the partial dissolution of inherent precipitates.

The microstructure of 316LN SS–weld interface is shown in Fig. 6. The presence of delta ferrite is observed which may be attributed to Creq/Nieqof 316LN steel. Lin [31] reported the presence of delta ferrite during ATIG of 316L. Further, the fraction of delta ferrite can be confirmed by SEM analysis.

The hardness profile of different zones of samples welded using TIG and ATIG with Co_3O_4 and TIO_2 is shown in Fig. 7. The higher hardness in weldment of TIG and ATIG with flux TiO_2 compared to base metal may result from martensitic transformation. This happens due to

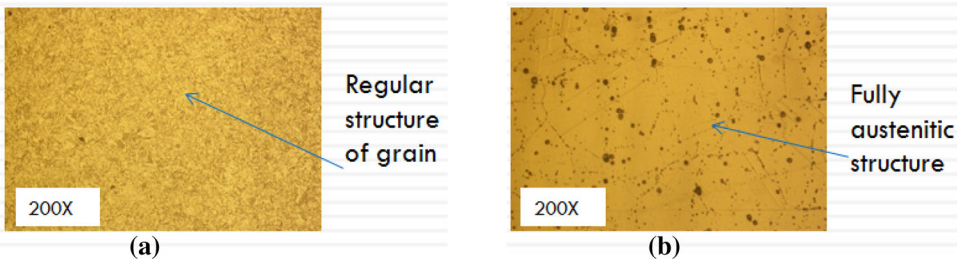

Fig. 5 Microstructure of base metal at 200X magnification **a** LAFM steel **b** 316LN stain less steel

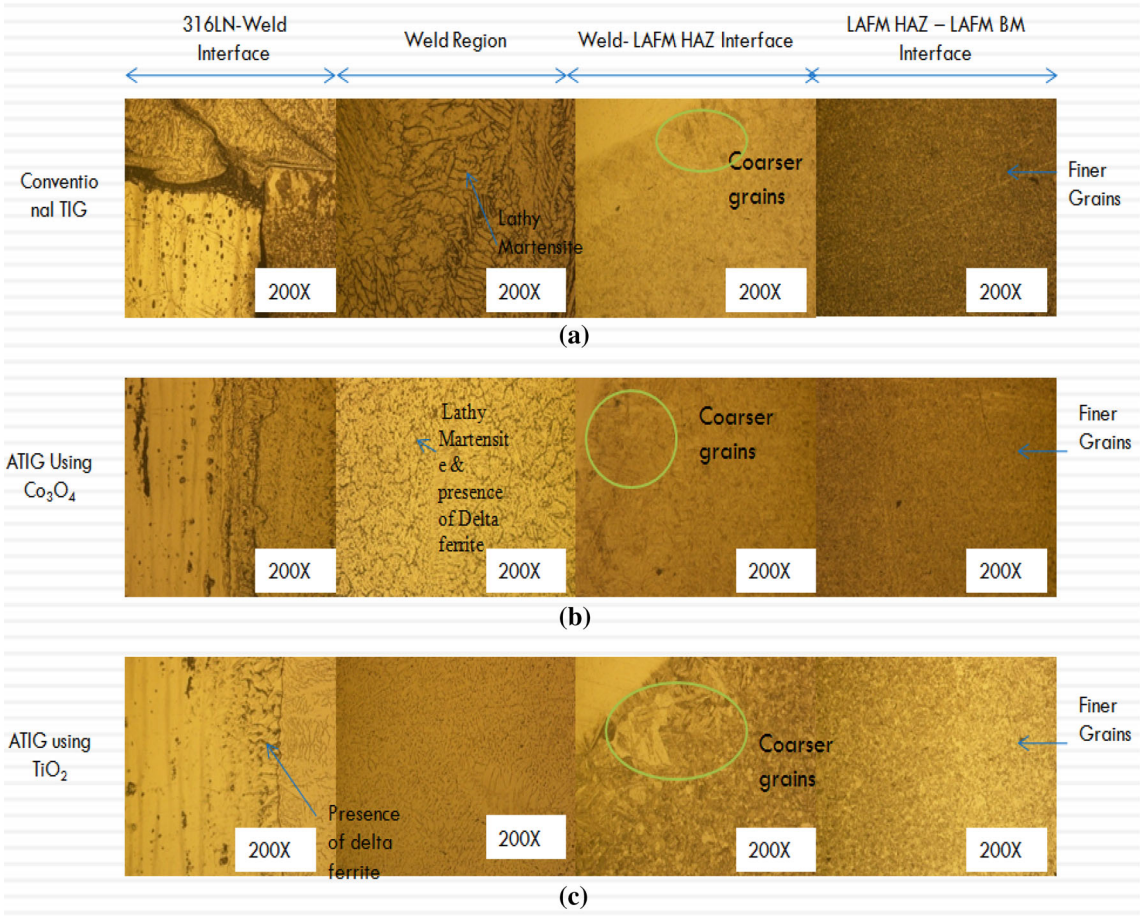

Fig. 6 Optical microstructure of different zones of samples welded using **a** conventional TIG; **b** ATIG with Co_3O_4 flux; and **c** ATIG with TiO_2 observed at 200X

the faster cooling rate as a result of higher temperature gradients. In contrary to this, the hardness of ATIG with flux Co_3O_4 is observed to be low. This may be due to a higher portion of 316LN in Weldment and formation of delta ferrite. Base metal hardness is lower as compared to weldment and LAFM HAZ. This can be attributed to quenching and tempering effect in as-received condition as discussed in the previous section. The LAFM HAZ hardness is observed to be higher as compared to base metal due to a higher temperature gradient compared to the base metal. There is no significant change in the hardness of 316LN base metal and 316LN HAZ.

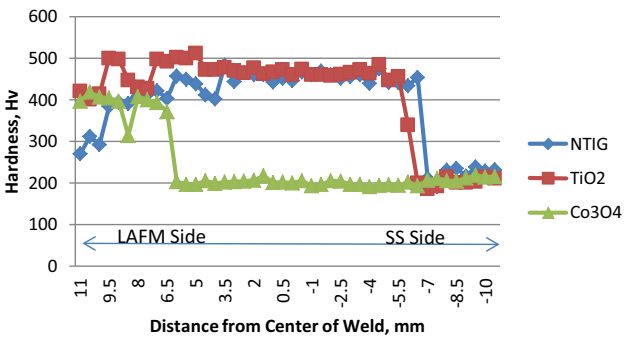

Fig. 7 Hardness profile of different locations covering all zones

4 Conclusions

In the present study, the ATIG welding process with five different oxide fluxes was utilized to make dissimilar weld joint between 316LN to LAFM steel. Its results were compared with the convention TIG welding experiment result. The effect of different fluxes was analyzed through visual inspection, macro- and microexamination, microhardness testing. Conclusions made from the above works are:

- The ATIG welding process can be successfully utilized for dissimilar welding of LAFM to 316LN steel using Co_3O_4 and TiO_2 fluxes.
- The surface appearance of TIG welded joints was more superior to ATIG. Excessive spatter was observed in ATIG with Co_3O_4. Also, a higher D/W ratio was observed in the case of ATIG welding using Co_3O_4 and TiO_2 Flux.
- An increase in arc voltage was reported in the case of ATIG welding using Co_3O_4 and TiO_2 Flux, which might increase peak temperature and support the presence of arc constriction mechanism.
- A dual mechanism, reverse Marangoni and arc constriction, was present in the case of ATIG welding using Co_3O_4 and TiO_2 flux. There was complete absence of arc constriction mechanism in the case of other three fluxes.
- Lathy martensitic structure was observed in weld metal except in the case of oxide flux Co_3O_4. A range of coarse to fine structure was observed from LAFM HAZ to LAFM base metal. There was no significant change in the microstructure of 316LN base metal and 316LN HAZ.
- A maximum hardness of 446 HV and 450 HV was observed in TIG welded sample and ATIG with the use of TiO2 Flux, respectively. However, hardness in the weld of ATIG with the use of Co_3O_4 was nearly similar to that of 316LN HAZ and base metal of 220 HV.

Acknowledgements Authors would like to thank PDPU, Gandhinagar, for the utilization of the ATIG welding facility available at Welding Research Laboratory, and SoT and GEC, Gandhinagar, for their microhardness testing facility. Authors would also like to extend their gratitude to the kind and sincere reviewers for enhancing the quality of papers.

References

1. Kurtz R J, Alamo A, Lucon E, Huang Q, Jitsukawa S, Kimura A, Klueh R, Odette G R, Petersen C, and Sokolov M A, *J Nucl Mater* **386** (2009) 411.
2. Activivty D R D, in *IFERC,* Rokasho, Aomori Japan (2013)
3. Aubert P, Tavassoli F, Rieth M, Diegele E, and Poitevin Y, *J Nucl Mater* **417** (2011) 43.
4. Manugula V L, Rajulapati K V, Madhusudhan Reddy G, Mythili R, and Bhanu Sankara Rao K, *Metall Mater Trans A* **48** (2017) 3702.
5. Manugula V L, Rajulapati K V, Reddy GM, Rajendra Kumar E, and Rao K B, *Sci Technol Weld Join* **23** (2018) 666.
6. Albert S K, Das C R, Sam S, Mastanaiah P, Patel M, Bhaduri A, Jayakumar T, Murthy C, and Kumar R, *Fus Eng Des* **89** (2014) 1605.
7. Vora J J, in *Advances in Welding Technologies for Process Development*, (eds) Vora J J, and Badheka V J, vol 1. CRC Press, Taylor and Francis (2019), p 23. https://doi.org/10.1201/9781351234825-11
8. Vora J J (2017) Development of Flux Assisted Tungsten Inert Gas Welding Process for Low Activation Ferritic Martensitic Steel. Pandit Deen Dayal Petroleum University, Gandhinagar.
9. Vaishnani S, Sadhu J, Suthar S, Vora J J, and Patel V (2017), Paper presented at the *4th International Conference on Industrial Engineering* (ICIE 2017), Surat, Gujarat.
10. Naik A, Kundal D, Suthar S H, Vora J J, Patel V V, Das S, and Patel R, in *Technology Drivers: Engine for Growth Proceedings of the 6th NIRMA University International Conference on Engineering (NUICONE 2017), November 23–25, 2017, Ahmedabad, India*, (eds) Mahajan A, Modi B A, and Patel P, vol 1. CRC press, Taylor & Francis (2018), p 243.
11. Raj B, Vijayalakshmi M, Sivaprasad P, Panigrahi B, and Amarendra G, *Indira Gandhi Centre for Atomic Research Kalpakkam* (2008).
12. Vijaya L, Manugula K V R, Madhusudhan Reddy G, Mythili R, and Bhanu Sankara Rao K, *Mater Des* **92** (2016) 200.
13. Vidyarthy R, Kulkarni A, and Dwivedi D, *Mater Sci Eng A* **695** (2017) 249
14. Fuzeau J, Vasudevan M, and Maduraimuthu V, *Trans Indian Inst Met* **69** (2016) 1493.
15. Hicken G K, Campbell R D, Daumeyer G J, Madigan R B, Young B, and Marburger S J, In: *AWS Welding Handbook*, American Welding Society, USA (1997), p 74.
16. Shyu S, Huang H, Tseng K, and Chou C, *J Mater Eng Perform* **17** (2008) 193.
17. Nayee S G, and Badheka V J, *J Manuf Process* **16** (2014) 137.
18. Tseng K-H, and Hsu C-Y, *J Mater Process Technol* **211** (2011) 503.
19. Vora J J, and Badheka V J, *Trans Indian Inst Met* **69** (2016) 1755.
20. Vora J J, and Badheka V J, *J Manuf Process* **20** (2015) 224.
21. Vora J J, and Badheka V J, *J Manuf Process* **25** (2017) 85. https://doi.org/10.1016/j.jmapro.2016.11.007.
22. Vora J J, and Badheka V J, *Int J Adv Mech Automob Eng* **3** (2016) 5. http://dx.doi.org/10.15242/IJAMAE.AE0316011.
23. Dhandha K H, and Badheka V J, *J Manuf Process* **17** (2015) 48.
24. Arivazhagan B, and Vasudevan M, *J Manuf Process* **16** (2014) 305.
25. Chern T-S, Tseng K-H, and Tsai H-L, *Mater Des* **32** (2011) 255.
26. Kumar V, Lucas B, Howse D, Melton G, Raghunathan S, and Vilarinho L, in JOM-15-*Fifteenth International Conference on the Joining of Materials* (2009), p 1.
27. Kou S, Limmaneevichitr C, and Wei P S, *Weld J* **90** (2011) 229-S
28. Berthier A, Paillard P, Carin M, Valensi F, and Pellerin S, *Sci Technol Weld Join* **17** (2012) 609.
29. Mills K C, Keene B J, Brooks R F, and Shirali A, *Philos Trans R Soc Lond A* **356** (1998) 911.
30. Yang C, Lin S, Liu F, Wu L, and Zhang Q, *J Mater Sci Technol* **19** (2003) 225.
31. Lin K-H, and Ta P-Y, *Materials* **7** (2014) 4755.
32. Lucas W, *Weld Met Fabr* **68** (2000) 7.